DOI: 10.61782/fa.2023.0389

forum acusticum 2023

ON NON-REFLECTIVE BOUNDARIES FOR OUTDOOR SOUND PROPAGATION USING THE DISCONTINUOUS GALERKIN METHOD

Sophia Julia Feriani[1*] **Allan P. Engsig-Karup**[2]
Finnur Pind[3] **Matthias Cosnefroy**[3] **Cheol-Ho Jeong**[1]
[1] Acoustic Technology, Department of Electrical and Photonics Engineering, Technical University of Denmark, Denmark
[2] Scientific Computing, Department of Applied Mathematics and Computer Science, Technical University of Denmark, Denmark
[3] Treble Technologies, Hafnartorg, Kalkofnsvegur 2, 101 Reykjavík, Iceland

ABSTRACT

In environmental acoustics, sound propagates in open air and can be mathematically modelled in terms of a semi-infinite domain. The calculations for accurate numerical solutions for outdoor acoustics are computationally heavy when the chosen computation domain is large enough to fulfil the Sommerfeld radiation condition. To lower the computational cost, the domain must therefore be truncated to not significantly impact the numerical solution inside the domain and allow outgoing acoustic waves to leave the domain undisturbed. Various radiation conditions (sometimes considering the wind) have been developed to achieve this goal such as the Perfectly Matched Layer method. The aim of this study is to compare the accuracy of different non-reflecting boundaries using the high-order nodal discontinuous Galerkin finite element method (DG-FEM) for the case of an acoustic pulse propagating in a static and moving medium in an unstructured mesh. For each boundary treatment, the tunable parameters of the methods are defined to balance accuracy and computational cost.

Keywords: *Environmental acoustics, non-reflective boundaries, nodal discontinuous Galerkin finite element method, perfectly matched layer*

**Corresponding author*: *sjufe@dtu.dk.*

1. INTRODUCTION

When modeling outdoor sound propagation, the acoustic waves travel in a semi-infinite domain. Therefore, the computational domain in numerical simulations must be truncated at an artificial limit that acts as a non-reflective boundary for the outgoing acoustic waves. The definition of this boundary should allow those waves to leave the domain undisturbed and not significantly impact the numerical solution inside the domain of interest.

Two strategies can be implemented to address this challenge: non-reflecting boundary conditions (NRBC) and layers (NRBL). NRBC have the advantage of being computationally efficient but have poor accuracy. The most widely used NRBC are the ones from Bayliss-Turkel [1] and Engquist-Majda [2]. Higher-order NRBC, pioneered by Collino [3], are more competitive in terms of accuracy but they are challenging to implement, and add non-negligible extra computation costs. The NRBL strategy consists of adding extra grid points at the edge of the grid, creating a layer where the waves are artificially decayed quicker than inside the original domain. In this layer, the waves can be dampened [4], the grid can be stretched [5], or the waves can be accelerated towards the outer edge to slow down the reflections [6]. However, those techniques are not flexible enough to accommodate more complex study cases (moving medium, wide range of frequencies, curvilinear grid, etc.).

The Perfectly Matched Layer (PML) technique was introduced in the mid-90s for the Maxwell equations [7]. It has been a popular sub-field of research since it solves most of the flexibility issues of previous NRBL techniques

and is more accurate than NRBC. The stability and well-posedness of the PML have been proved [8–10], and the technique is used in various problems, including outdoor acoustics. Hu, in particular, focused on applying PML to the time-domain wave equation in static and moving mediums [11–14].

PML is a complex change of variable in the frequency domain, which dampens the perturbation modes inside the layer and limits the generation of spurious reflections inside the domain of interest. The parameters that define the PML are the thickness of the layer, the refinement of its mesh, and the absorption function. To improve accuracy, the first two parameters presuppose an increase in computation, so the last parameter has been more thoroughly studied to evaluate an optimal definition of the absorption function acting on the waves entering the PML domain [15–17]. The thickness of the PML has been less studied because it is case-dependent.

In this paper, we will discuss non-reflective boundaries in the time-domain wave equation for outdoor acoustics using the discontinuous Galerkin finite element method (DG-FEM) [18]. The accuracy in the discrete domain for different non-reflective boundaries are compared. We then focus on the PML technique in a static and a moving medium and characterize the different types of reflection of the acoustic waves polluting the domain of interest.

2. METHOD

2.1 Governing equations and numerical scheme

The acoustic wave equations describe the propagation of sound in the atmosphere in the time domain as follows: for $(x, y) \in R^2$ and $t \leq 0$:

$$\frac{\partial p}{\partial t} + \rho_0 c^2 \nabla . \boldsymbol{v} + \boldsymbol{v_0} \cdot \nabla p = \rho_0 c^2 \boldsymbol{Q} \tag{1}$$

$$\frac{\partial \boldsymbol{v}}{\partial t} + \frac{\nabla p}{\rho_0} + (\boldsymbol{v_0} \cdot \nabla)\boldsymbol{v} + (\boldsymbol{v} \cdot \nabla)\boldsymbol{v_0} = \frac{\boldsymbol{F}}{\rho_0} \tag{2}$$

with $p(x, y, t)$ the acoustic pressure in Pa, $\boldsymbol{v}(x, y, t) = (v_x, v_y)$ the particle velocity vector in m/s, at time t and location (x, y) for the case of two-dimensional sound propagation. $\boldsymbol{v_0} = (v_{x,0}, v_{y,0})$ is the mean wind in m/s. The density of air $\rho_0 = 1.2\ kg/m^3$ is considered constant at and the speed of sound is set to $c = 343\ m/s$. $\boldsymbol{Q}$ and $\boldsymbol{F}$ correspond to potential mass sources and external forces and are considered null in this study. Those set of equations can be condensed into the following matrix form:

$$\frac{\partial \boldsymbol{u}}{\partial t} + \boldsymbol{A}\frac{\partial \boldsymbol{u}}{\partial x} + \boldsymbol{B}\frac{\partial \boldsymbol{u}}{\partial y} + \boldsymbol{C}\boldsymbol{u} = 0 \tag{3}$$

The equations are solved using the DG-FEM [18]. For the numerical flux that allows communication between elements, an upwind flux is constructed derived from the eigenstructure of the model equations [19].

The approximated solution is interpolated at interpolation nodes chosen as the Legendre-Gauss-Lobatto quadrature points. It is advanced in time using a fourth order explicit Runge-Kutta scheme with a time-step chosen small enough to ensure a discretely stable scheme and that the time-step error can be neglected (Courant-Friedrichs–Lewy number equal to 0.75).

At initial time, the sound pressure spatial distribution is a Gaussian pulse (Eqn. (4)) of width $\alpha = 0.1$ m, centered around the point source $S(x_s = 0, y_s = 0)$ as in Fig. 1:

$$p(x, y, 0) = exp\left(-ln(2)\frac{(x - x_s)^2 + (y - y_s)^2}{\alpha^2}\right) \tag{4}$$

It translates to a peak frequency of around 640 Hz and correspond to roughly 6.5 points per wavelength at this peak frequency. The particle velocities in the x- and y-directions are null: $\boldsymbol{v}(x, y, 0) = \boldsymbol{0}$.

The domain of interest Ω is a 5 m-by-5 m mesh centered in $(0, 0)$ and containing $K = 582$ triangular elements as in Fig. 1. For the case of NRBL, an extra layer Ω_{PML} at the periphery of Ω is added and has a width of δ. Three widths δ are considered: 1m, 2.5m and 7.5m.

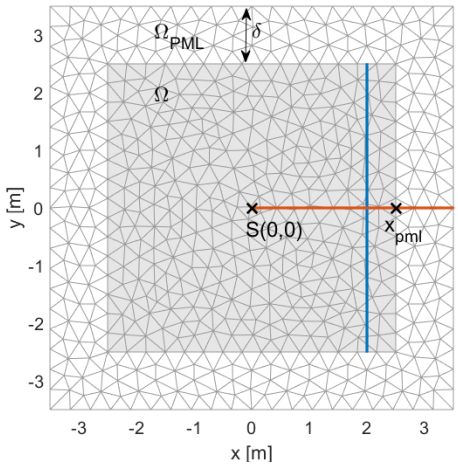

Figure 1. Notation of the mesh. In blue is represented the Γ line along which the energy is evaluated and in orange is represented the Γ line along which the energy is evaluated.

2.2 Non-reflecting Boundary

2.2.1 *Non-reflecting Boundary Conditions*

Three types of non-reflective boundary conditions are tested:

- Impedance-based boundary condition where the outer boundary of the mesh has an impedance of $Z = \rho_0 c$.
- Impedance-based with angular correction boundary condition where the impedance has been corrected to account for the angle of incidence of the wave hitting the outer boundary of the mesh
- Zero-th order absorbing boundary condition where the external characteristics are zero when calculating the flux over the outer edge of the triangular elements of the mesh bordering Ω.

2.2.2 *Non-reflecting Boundary Layers*

Two types of non-reflective boundary layers methods are tested and implemented on Ω_{PML}:

- Grid stretching where the x- and y-derivatives of the equations are stretched linearly.
- Simple dampening where the term $(\sigma_x + \sigma_y)u$ is added to the left side of Eqn. (3)) with $\sigma_x = c\frac{x-x_{PML}}{\delta}$ and $\sigma_y = c\frac{y-y_{PML}}{\delta}$ only in the extra layer (see Fig. 1 for the notation).

A reflective boundary condition is imposed at the end of the layer.

2.2.3 *Perfectly matched layer (PML)*

The PML method corresponds to a complex coordinate stretching in the frequency domain. This transformation is implemented inside Ω_{PML} in order to absorb the outgoing acoustic energy leaving the domain and without creating spurious reflections inside Ω (i.e. the perfectly matched layer).
With the following change of variable, the PML can be fully described in the static case:

$$x \to \left(1 + \frac{i\sigma_x}{\omega}\right) x \text{ and } y \to \left(1 + \frac{i\sigma_y}{\omega}\right) y \tag{5}$$

where σ_x and σ_y are the absorption functions and ω is the angular frequency. After introducing the auxiliary variable $\boldsymbol{q}$, the following PML equations are solved in Ω_{PML} for the case of a static domain [12]:

$$\frac{\partial \boldsymbol{u}}{\partial t} + \boldsymbol{A}\frac{\partial \boldsymbol{u}}{\partial x} + \boldsymbol{B}\frac{\partial \boldsymbol{u}}{\partial y} + \sigma_y \boldsymbol{A}\frac{\partial \boldsymbol{q}}{\partial x} + \sigma_x \boldsymbol{B}\frac{\partial \boldsymbol{q}}{\partial y} + (\sigma_x + \sigma_y)\boldsymbol{u} + \sigma_x\sigma_y \boldsymbol{q} = 0 \tag{6}$$

$$\frac{\partial \boldsymbol{q}}{\partial t} = \boldsymbol{u} \tag{7}$$

In the case of a uniformly moving medium, the following PML equations are solved in Ω_{PML} [12]:

$$\frac{\partial \boldsymbol{u}}{\partial t} + \boldsymbol{A}\frac{\partial \boldsymbol{u}}{\partial x} + \boldsymbol{B}\frac{\partial \boldsymbol{u}}{\partial y} + \sigma_y \boldsymbol{A}\frac{\partial \boldsymbol{q}}{\partial x} + \sigma_x \boldsymbol{B}\frac{\partial \boldsymbol{q}}{\partial y} + (\sigma_x + \sigma_y)\boldsymbol{u} + \sigma_x\sigma_y \boldsymbol{q} + \frac{\sigma_x M_x}{1 - M_x^2}\boldsymbol{A}(\boldsymbol{u} + \sigma_y \boldsymbol{q}) = 0 \tag{8}$$

$$\frac{\partial \boldsymbol{q}}{\partial t} = \boldsymbol{u} \tag{9}$$

where $M_x = \frac{v_{x,0}}{c}$ is the subsonic Mach number in medium with a mean flow of $\vec{v_x} = v_{x,0}\vec{e_x}$. This study tests only the cases where Mach numbers $M_x > 0$ and $M_y = 0$, which correspond to the situation where wind blowing uniformly and horizontally across the full domain.

At the termination of the PML, a perfectly reflective boundary condition is imposed to isolate the absorbing performance of the PML.

Different profiles of absorption $\sigma_x(x)$ and $\sigma_y(y)$ are tested. They are defined as a polynomial function of space in Ω_{PML} and null in Ω:

$$\sigma_x = \sigma_0 \left(\frac{x - x_{PML}}{\delta}\right)^n \text{ and } \sigma_y = \sigma_0 \left(\frac{y - y_{PML}}{\delta}\right)^n \tag{10}$$

where $n = \{0, 1, 2, 3\}$ which corresponds to a constant, linear, quadratic, and cubic absorption profile, respectively. $\sigma_0 \geq 0$ is the absorption factor in s^{-1} and is a multiple M of the speed of sound c: $\sigma_0 = M \times c$ with $M \geq 0$.

In theory, the PML absorbs the exact wave equation if the absorption factor is high enough. "Round-trip" reflections can appear if the PML is not absorbent enough (small σ_0). This type of reflections is the original wave bouncing off the perfectly reflective boundary at the end of the PML and carrying energy back into Ω.
However, the absorption factor σ_0 cannot take large values either because the discretization with DG-FEM (or other numerical schemes) inevitably introduces an approximation in the solution which creates spurious reflections. This type of reflections can be called "transient" reflections and can be curtailed by slowly varying the PML zone absorption profile and/or widening the PML.

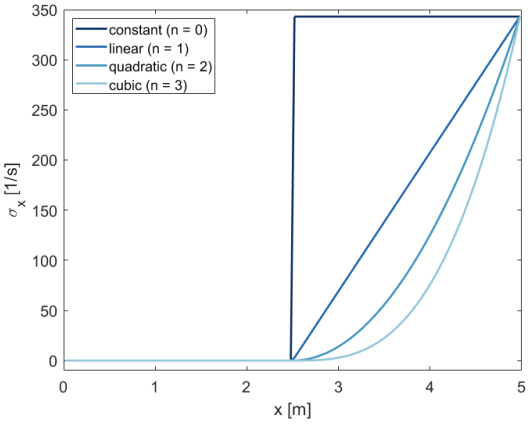

Figure 2. Absorption profile $\sigma_x(x)$ in the $x > 0$ part of the domain for $\sigma_0 = 1 \times c$ and a PML width of δ = 2.5m.

Therefore, a compromise needs to be reached between the different PML parameters:

- the absorption factor σ_0 in Eqn. (10),
- the absorption function profile by choosing n in Eqn. (10),
- the discretization error of the scheme by choosing N and K in the DG-FEM scheme,
- the width of the PML δ,
- the computational time and storage.

To quantify the error produce by those choices, the relative energy reflected and the time average of the L_∞-norm on the pressure are evaluated.

2.3 Error definitions

2.3.1 Relative energy

For the round-trip reflection, we are interested in assessing the amount of energy coming back into Ω. The energy of the acoustic wave along a line Γ is defined as:

$$E_\Gamma(\sigma_0, t) = \left[\int_\Gamma \frac{1}{2}\frac{1}{\rho_0 c^2}p^2 - \frac{1}{2}\rho_0 \boldsymbol{v}^2 \, d\gamma\right]^{1/2} \tag{11}$$

where Γ is chosen as the path of normal incidence to the PML in Fig. 1.

The relative energy along the same line Γ and time t is defined as the ratio between the case where the absorption is positive: $\sigma_0 > 0$, and the case where no PML treatment has been applied: $\sigma_0 = 0$.

$$\xi_\Gamma(\sigma_0, t) = \frac{E_\Gamma(\sigma_0, t)}{E_\Gamma(0, t)} \tag{12}$$

For the static cases, the relative energy is calculated at time $t_R = \frac{x_{PML}+2\delta}{c}$ and since the problem is symmetric only the positive line is considered. At t_R, $E_\Gamma(\sigma_0, t_R)$ corresponds to the energy of the wave as it leaves the PML after travelling back and forth the width of the PML (2δ). For the moving medium cases, the relative energy is calculated at time $t_R = \frac{x_{PML}+2\delta}{c(1+M_x)}$ for the downwind case (positive x).
$\xi_\Gamma(\sigma_0, t_R)$ is the relative energy reflected. When $\xi_\Gamma(\sigma_0, t_R)$ tends to 1, the PML is not absorbing the wave enough and the full domain ($\Omega \cup \Omega_{PML}$) acts like a close domain. Whereas, when $\xi_\Gamma(\sigma_0, t_R)$ tends to zero, the PML performs well enough so that negligible energy from round-trip reflections is coming back to pollute Ω.

2.3.2 L_∞-norm on the pressure

A highly non-reflective boundary is a boundary that lets negligible spurious reflections coming back into the domain of interest. It can be evaluated by comparing the pressure in a domain including a non-reflective boundary treatment (NRBC or NRBL) with a reference pressure.
The reference pressure p_{ref} is obtained by simulating the same setup over a very large mesh and without non-reflecting boundary treatment.

The time average of L_∞-norm on the pressure is defined as:

$$\langle L^p_\infty(t)\rangle = \frac{1}{T}\int_0^T \max_{(x,y)\in\Gamma}(|p - p_{ref}|)\; dt \tag{13}$$

where Γ is the line along which the norm is calculated. In the study, the L_∞-norm is evaluated at $x = 2\ m$ inside Ω in order to capture the pressure difference with the reference case close to the PML and it correspond to the blue line in Fig. 1. T is the simulation time. It is chosen long enough for the pressure to decay under 20 μPa (perceptual threshold).

3. RESULTS

3.1 Static medium

Figure 3 and Figure 4 compare the accuracy of the NRBC and NRBL (including the PML case) considered over the

polynomial order N of the DG-FEM scheme using the time average of the L_∞-norm on the pressure. The dashed line corresponds to the perceptual level (20 μPa).

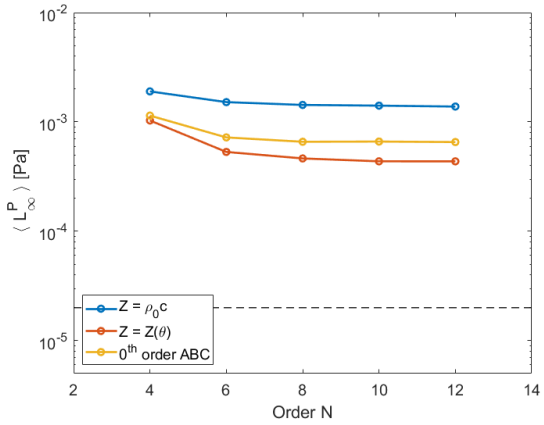

Figure 3. L_∞-norm on the pressure along the blue line for three NRBC.

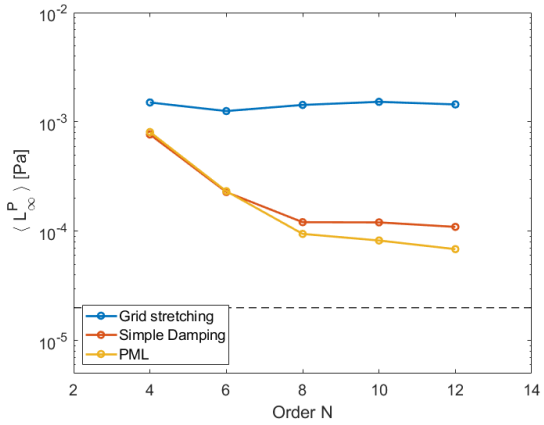

Figure 4. L_∞-norm on the pressure along the blue line for two NRBL and PML.

Figure 5 compares the magnitude of the round-trip reflections of the PML over a range of absorption factor σ_0 using the relative energy reflected with $N = 10$. Four absorption profiles are considered $n = \{0, 1, 2, 3\}$ and they all reach the same maximum absorption of σ_0 at the end of the PML ($x_{PML} + \delta$).

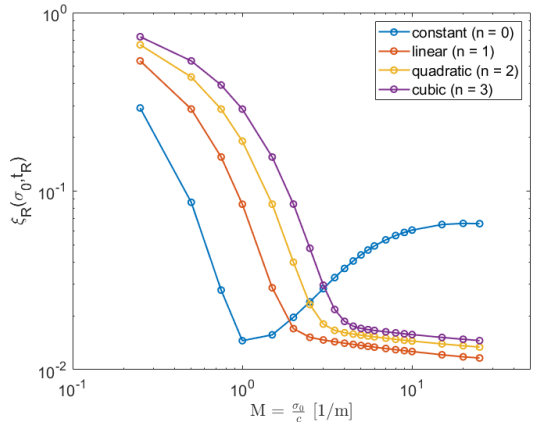

Figure 5. Relative energy reflected along the orange line for four different absorption profiles with $N = 10$.

Figure 6 compares the magnitude of the transient reflections from the PML for different widths of PML (1 m, 2.5 m and 7.5 m) using the time average of the L_∞-norm on the pressure with $N = 10$. The case of linear absorption ($n = 1$) is chosen because it is the most uniformly varying profile.

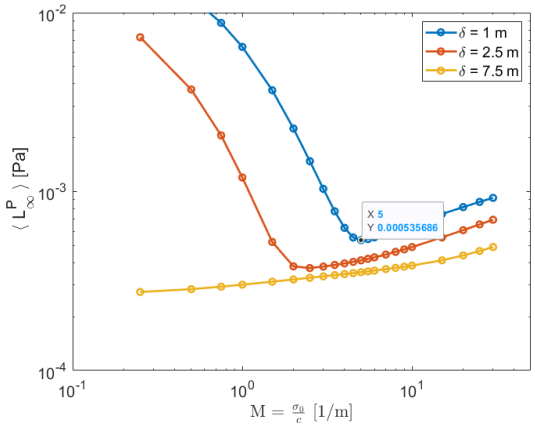

Figure 6. L_∞-norm on the pressure over the absorption factor along the blue line for three different widths of PML.

3.2 Moving medium

For this section, a linear absorption profile is again chosen. The PML has a width of $\delta = 2.5\ m$ and the relative energies reflected are evaluated at their respective time t_R for different Mach number $M_x \geq 0$. The relative energy reflected is evaluated on the same line as for the static case (equivalent to $M_x = 0$) which corresponds to the downwind side in Fig. 7.

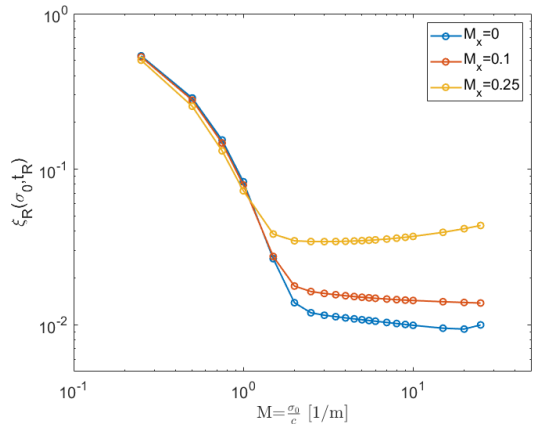

Figure 7. Relative energy reflected along the orange line for the case of moving medium and the static case.

4. DISCUSSION

Figure 3 and Figure 4 show that PML has better accuracy compared to the considered NRBC and NRBL, especially at high order. The existing literature corroborates these findings which justifies the extensive research on the PML method in the last decades over other types of non-reflecting boundaries.

As expected, the round-trip reflections magnitude decreases fast as the absorption factor starts to increase from zero to higher absorption factors σ_0 in Fig. 5: the relative energy reflected $\xi_\Gamma(\sigma_0, t_R)$ start from 1 when no PML is imposed ($M = 0\ m^{-1}$) and decreases rapidly to around 2×10^{-2} for all absorption profiles. For the linear, quadratic and cubic cases ($n \in \{1, 2, 3\}$), $\xi_\Gamma(\sigma_0, t_R)$ stops decreasing as rapidly after different absorption factors are reached (M equal to 2, 3 and 3.5, respectively) and ultimately stabilises around 1×10^{-2}. This stems from the nodal DG-FEM discretization scheme: for a fixed PML width, the jump of absorption gets higher and higher as the absorption factor σ_0 increases which introduced a numerical error. However, for the constant case ($n = 0$), the relative energy reflected even increases once M reaches $1\ m^{-1}$ and grow up to 6×10^{-2} in the absorption range considered. The discontinuity in the absorption profile of the constant case is experienced by the waves at the entrance of the PML so at high absorption factor σ_0 or high M, the PML acts like a wall and reflects part of the wave back to Ω.

To quantify the transient reflections coming back to Ω, Fig. 6 shows the time average of the L_∞-norm on the pressure over the absorption factor on a line at $x = 2\ m$. Transient reflections are minimal when the absorption factor is small since the jumps of absorption in the PML in the discrete scheme are also small. When the absorption factor is large, more energy is reflected inside Ω. The PML with a width of 1 m and 2.5 m present a minimum time average L_∞-norm of 3.7×10^{-4} at $M = 2.5\ m^{-1}$ and 5.3×10^{-4} at $M = 5\ m^{-1}$, respectively. The largest PML where $\delta = 7.5\ m$ is too wide to get noticeable reflection back to Ω. However, a wide PML implies longer computational time. Therefore, a compromise needs to be made where, for a fixed absorption profile, the PML width is adjusted according to the error tolerated.
In this study, the boundary conditions at the termination of the PML are perfectly reflective so that only the absorption through the PML is considered. Better accuracy should be expected if the end of the PML is a NRBC.

In the case of moving medium in Fig. 7, the downwind wave reaches the PML earlier than the wave in a static medium. The relative energies reflected at different Mach numbers for low M are comparable in the Mach range considered. However, the relative energy reflected $\xi_\Gamma(\sigma_0, t_R)$ starts decreasing less quickly at a smaller M for fast moving medium: $M = 1.5\ m^{-1}$ for a Mach number of 0.25 and $M = 2\ m^{-1}$ for a Mach number of 0.1 and 0. The error then stabilises to around 1×10^{-2}, 1.5×10^{-2} and 3.5×10^{-2} for a Mach number of 0, 0.1 and 0.25, respectively. Indeed, the absorption factor being related to the speed of sound c, the effect of a jump in absorption is felt earlier by the downwind wave.

5. CONCLUSION

The PML method has been a popular method in the last decades to deal with non-reflecting boundary because it is easy to implement, relatively accurate and flexible to multiple situations (different frequencies, angle of incidence, moving medium). In the case of outdoor acoustics, this study showed that PML is still an interesting choice when the problem is discretized using the nodal DG-FEM method. This method was used to implemented different types of non-reflecting boundaries including PML. Nevertheless, the PML parameters need to be determined carefully to be effective. The absorption needs to be strong enough to fulfill its purpose but also weak and gradual enough to not generate spurious reflections created from the discretization. Through the evaluation of the reflected energy and the L_∞-norm on the pressure, it was concluded that for all absorption functions, the performance of the PML improves when the absorption factor grows, but only until a certain threshold. After which, the performance plateaus out or, worst, it deteriorates.
More investigation needs to be done to generalize those findings for any PML width in static medium as well as in moving medium.

6. ACKNOWLEDGMENTS

The authors would like to thank Fernando Javier Canalejo Vicedo for his contribution to this work regarding different types of non-reflecting boundaries.

7. REFERENCES

[1] A. Bayliss and E. Turkel, "Radiation boundary condition for wave-like equations," *Communications on Pure and Applied Mathematics*, vol. 33, pp. 707 – 725, 11 1980.

[2] B. Engquist and A. Majda, "Radiation boundary conditions for acoustic and elastic wave calculations," *Communications on Pure and Applied Mathematics*, vol. 32, pp. 313 – 357, 05 1979.

[3] F. Collino, "High order absorbing boundary conditions for wave propagation models. straight line boundary and corner cases," *Proc. 2nd Int. Conf. on Mathematical Numerical Aspects of Wave Propagation*, 01 1993.

[4] M. Israeli and S. A. Orszag, "Approximation of radiation boundary conditions," *Journal of Computational Physics*, vol. 41, no. 1, pp. 115–135, 1981.

[5] D. Appelö and T. Colonius, "A high-order super-grid-scale absorbing layer and its application to linear hyperbolic systems," *Journal of Computational Physics*, vol. 228, pp. 4200–4217, 06 2009.

[6] T. Shlomo and N. Douglas, "An absorbing buffer zone technique for acoustic wave propagation," *33rd Aerospace Sciences Meeting and Exhibit*, 01 1995.

[7] J.-P. Berenger, "A perfectly matched layer for the absorption of electromagnetic waves," *Journal of Computational Physics*, vol. 114, no. 2, pp. 185–200, 1994.

[8] S. Abarbanel and D. Gottlieb, "A mathematical analysis of the pml method," *Journal of Computational Physics*, vol. 134, no. 2, pp. 357–363, 1997.

[9] J. Hesthaven, "On the analysis and construction of perfectly matched layers for the linearized euler equations," *Journal of Computational Physics*, vol. 142, 08 1997.

[10] D. Appelö, T. Hagstrom, and G. Kreiss, "Perfectly matched layers for hyperbolic systems: General formulation, well-posedness, and stability," *SIAM Journal of Applied Mathematics*, vol. 67, pp. 1–23, 01 2006.

[11] F. Hu, "On absorbing boundary conditions for linearized euler equations by a perfectly matched layer," *Journal of Computational Physics*, vol. 129, 11 1996.

[12] F. Hu, "A stable, perfectly matched layer for linearized euler equations in unsplit physical variables," *Journal of Computational Physics*, vol. 173, pp. 455–480, 11 2001.

[13] F. Q. Hu, "A perfectly matched layer absorbing boundary condition for linearized euler equations with a non-uniform mean flow," *Journal of Computational Physics*, vol. 208, no. 2, pp. 469–492, 2005.

[14] S. Parrish and F. Hu, "Pml absorbing boundary conditions for the linearized and nonlinear euler equations in the case of oblique mean flow," *International Journal for Numerical Methods in Fluids*, vol. 60, pp. 565 – 589, 06 2009.

[15] F. Collino and P. Monk, "Optimizing the perfectly matched layer," *Computer Methods in Applied Mechanics and Engineering*, vol. 164, pp. 157–171, 10 1998.

[16] A. Modave, E. Delhez, and C. Geuzaine, "Optimizing perfectly matched layers in discrete contexts," *International Journal for Numerical Methods in Engineering*, vol. 99, 08 2014.

[17] A. Bermudez, L. Hervella-Nieto, A. Prieto, and R. Rodríguez, "An optimal perfectly matched layer with unbounded absorbing function for time-harmonic acoustic scattering problems," *Journal of Computational Physics*, vol. 223, pp. 469–488, 05 2007.

[18] J. S. Hesthaven and T. Warburton, *Nodal Discontinuous Galerkin Methods: Algorithms, Analysis, and Applications*. Springer Publishing Company, Incorporated, 1st ed., 2007.

[19] A. Melander, E. Strøm, F. Pind, A. P. Engsig-Karup, C.-H. Jeong, T. Warburton, N. Chalmers, and J. S. Hesthaven, "Massively parallel nodal discontinous galerkin finite element method simulator for room acoustics," *Submitted to International Journal of High Performance Computing Applications*, 06 2020.